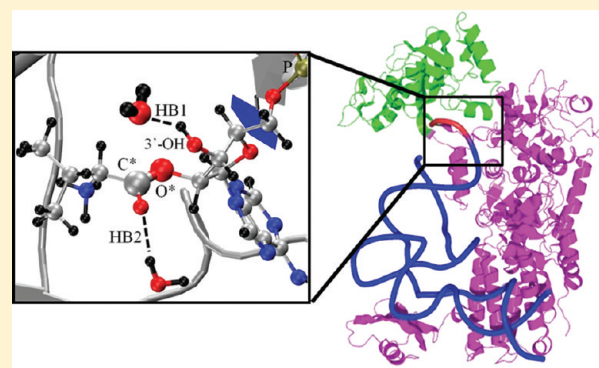


LeuRS Synthetase: A First-Principles Investigation of the Water-Mediated Editing Reaction

Mauro Boero^{*,†,‡}[†]Institut de Physique et Chimie des Matériaux de Strasbourg UMR 7504 CNRS-UDS, 23 rue du Loess, BP 43, F-67034 Strasbourg, France[‡]Research Center for Integrated Science, Japan Advanced Institute of Science and Technology (JAIST), 1-1 Asahidai, Nomi, Ishikawa 923-1292, Japan

ABSTRACT: Starting from the crystallographic structure of the *Thermus thermophilus* leucyl-tRNA (LeuRS) synthetase system and recent theoretical findings, our combined hybrid QM/MM and free energy metadynamics sampling approach shows that in the editing domain the enzymatic activity is initiated by the dissociation of a specific water molecule in proximity of the chemical bonds ($-C^*-O^*$) constituting the nucleotide binding of the tRNA to the leucyl protein. A crucial promoter of the reaction is the 3'-OH group of the cognate tRNA bound to the editing site of leucyl, which forms a stable hydrogen bond with this peculiar catalytic water molecule. We could identify two possible reaction mechanisms for the initial stage of the editing reaction: In one case the 3'-OH group of the cognate tRNA acts as a Lewis acid, and one of the protons of the catalytic water molecule becomes a temporarily shared proton between 3'-OH and this specific H₂O, thus helping its dissociation. The dissociation products OH⁻ and H⁺ attack the C* and O* atoms, respectively, thus promoting the C-O bond cleavage. In the second case, the 3'-OH group of the cognate tRNA drives, via its hydrogen bond, the catalytic water molecule toward the $-C^*-O^*$ bond, and the unoccupied LUMO state, located on top of this bond, becomes the electron acceptor for the dissociating water molecule. This promotes the reaction toward the same final product found in the former pathway, but without involving temporary proton transfers to 3'-OH.



1. INTRODUCTION

The aminoacyl-tRNA synthetases (aaRSs) is a large family of tRNA-binding proteins, amounting to more than 20,^{1–5} whose crucial roles are the translation of the genetic code with a high fidelity⁶ and the promotion of protein biosynthesis. The fundamental step in these processes is the catalytic attachment of the correct amino acid to its cognate tRNA (tRNA). An important member of this family, on which the present work is focused, is the leucyl-tRNA synthetase (LeuRS), belonging to the class I enzymes, whose catalytic core presents a typical Rossmann fold where the binding of the protein is realized with a nucleotide.⁷ This is a large monomeric enzyme composed of about 860 amino acid residues, as shown for the case of the *Escherichia coli*,⁸ and homologous to other members of the synthetases family, namely arginyl-tRNA (ArgRS), cysteinyl-tRNA (CysRS), isoleucyl-tRNA (IleRS), methionyl-tRNA (MetRS), and valyl-tRNA (ValRS) synthetases. The determination of the precise crystallographic structure of synthetases is particularly difficult, and only recently four of them could be resolved with appreciable accuracy: ArgRS,⁹ IleRS,¹⁰ ValRS,¹¹ and LeuRS.^{12,13}

The two pivotal roles of LeuRS are (i) the aminoacylation of the aliphatic amino acid leucine (Leu) for six isoacceptors tRNA types,^{12–15} differing in the specific anticodon region,¹⁶ and (ii) the editing (proofreading) reaction in which the tRNA is deacylated.^{17–21}

These two functions of LeuRS occur in two different regions of the Leu protein, as schematically sketched in Figure 1; these two active sites are separated by a distance equal to or larger than 34 Å, as determined from the crystal structure of the LeuRS in free archaeal *Pyrococcus horikoshii* with a 3.2 Å resolution.^{12,13} Although not extremely accurate because of the intrinsic difficulty in obtaining good samples of such a complicated system, such a resolution is sufficient to obtain reliable systems for computer simulations.

The aminoacylation reaction can be rationalized into two main steps: the formation of enzyme-bound aminoacyl-adenylate and the transfer of this activated amino acid to either the 2'- or 3'-OH group belonging to the ribose located at the 3'-terminal adenosine of the cognate tRNA. However, the mechanism responsible for the movement of the 3'-end segment of tRNA from the aminoacylation domain to the CP1 editing domain^{22,23} is still a matter of debate and largely unknown. The only information available to date is the identification of an intermediate state in which the tRNA 3'-end is partially relocated, as recently reported by the group of Yokoyama.¹³ For the sake of completeness, we

Received: July 22, 2011

Revised: September 15, 2011

Published: September 17, 2011

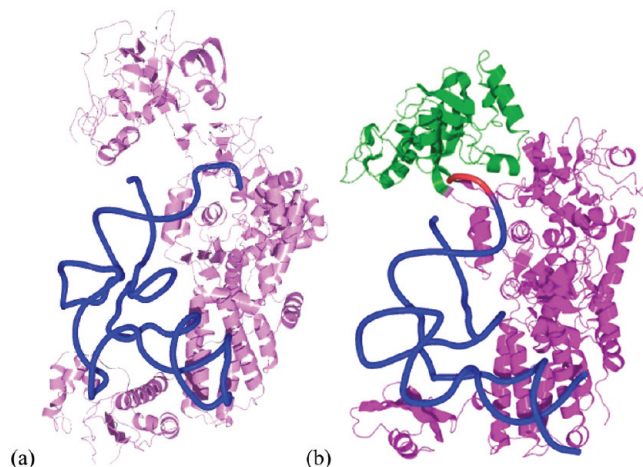


Figure 1. Ribbon model of the leucyl-tRNA. The aminoacylation conformation is shown in panel a where pink ribbons represent Leu and the blue tube tRNA. Panel b, on the right, shows the CP1 editing domain in green color, and the segment of tRNA attached to the Leu protein is evidenced in red.

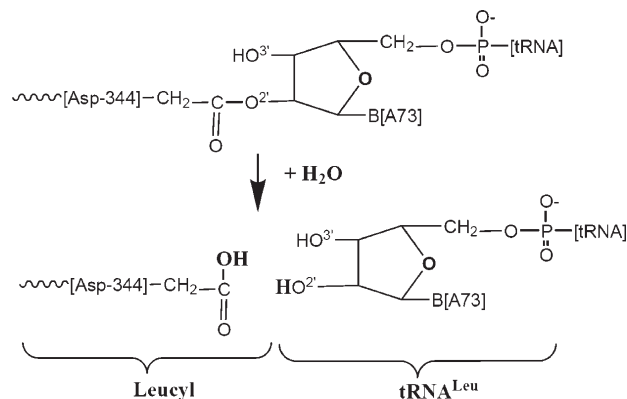
also have to mention that the aminoacylation activity in the yeast mitochondrial LeuRS can be hindered by its own C-terminal domain, adapting the system to a new role: the RNA splicing.²⁴ Such a role, accompanied by the suppression of the aminoacylation, should not be regarded as a negative feature since RNA splicing is also an essential activity in living organisms for the translation and manipulation of the genetic code.

One of the main features of a general member of the aaRSs family is the recognition of the anticodon region of their chaperone tRNA. At variance with this common trend, LeuRS does not recognize the anticodon of its cognate tRNA (tRNA^{Leu}). Instead, it recognizes the adenosine residue positioned at the site labeled as A73, which is expected to play a fundamental role in the conformational changes that tRNA^{Leu} undergoes upon binding to Leu.¹⁵ Hence, LeuRS synthetase catalyzes the tRNA^{Leu} leucylation in the vicinity, and most likely with the direct participation, of the 3'-OH group of the ribose of the 3'-terminal adenosine.^{24–28}

This specific aspect and the detailed investigation of reaction pathways and free energy landscapes associated with possible roles of the 3'-end nucleotide of tRNA is the main focus of the present work. We use as a reference system the *Thermus thermophilus* (*T. thermophilus*) LeuRS (Protein Data Bank accession code 2BYT) since it is the only system presently available, with a sufficiently accurate resolution, for which two possible alternative hydrolyses could be discriminated: pretransfer editing and post-transfer editing. Nonetheless, for the majority of the eubacterial LeuRSs, the pretransfer editing could not yet be detected to date, whereas confirmations exist concerning the post-transfer editing.^{29–31} The use of hybrid quantum mechanics/molecular mechanics reactive simulations allow us to inspect at an atomic level not accessible to experimental probes the hydrolysis reaction occurring during the post-transfer editing process. We have found that solvating water molecules can approach the active site, coming very close to the 3'-terminal of the tRNA^{Leu} where a

sequence of chemical bonds $\text{---C}=\text{O} \text{---C---O---C}^{\text{ribose}}$ represents the chemical connection of the cognate tRNA to the Leu protein. Water molecules coming in proximity of the C—O bond, upon dissociation, can take active part in the reaction mechanism by promoting

Scheme 1



the reaction $\text{---C}=\text{O} \text{---C---O}^{\text{ribose}} \text{---} + \text{H}_2\text{O} \rightarrow \text{---C}=\text{O} \text{---H} + \text{H---O---C}^{\text{ribose}}$ along two possible pathways, both involving an active participation of the 3'-OH group of the ribose of the 3'-terminal of tRNA^{Leu} and resulting in the general reaction scheme shown in Scheme 1.

In one case, the 3'-OH group participates by forming a rather stable hydrogen bond (H-bond) with the incoming water molecule, which is then kept close to the catalytic site. The first unoccupied electronic state results localized on the chemical bonds connecting the Leu protein and the tRNA^{Leu}, which become electron acceptors, thus becoming the driving force that favors the dissociation of the catalytic water molecule. In the second case, the 3'-OH undergoes temporary protonation and deprotonation processes that help the dissociation of the catalytic H₂O molecule and trigger the whole reaction. In both cases, identical final products and comparable activation energies show that these two alternative pathways are viable reaction mechanisms.

The LeuRS hydrolysis mechanisms depicted shows how this system can be seen as a novel hybrid RNA enzyme (ribozyme) catalyst with important consequences in the general genetic information transfer scenario and possible roles in the origin of life as a transitional form from the RNA world to the actual DNA-based world of living organisms.

2. COMPUTATIONAL APPROACH

2.1. The Target System. The LeuRS system used in the present set of simulations is identical to the one discussed in ref 28. Namely, it is taken from the X-ray crystallographic data of the LeuRS complex of the *T. thermophilus* as provided by Brookhaven Protein Data Bank (accession code 2BYT). We have to stress the fact that this crystallographic structure is missing the valine (Val) moiety attached to A76 and structural water molecules. This starting configuration was fully solvated by adding 49 587 water molecules, and the final system consists of the Leu protein and its cognate tRNA^{Leu}, amounting to 165 745 atoms—and including 99 counterions (98 Na⁺ and one Zn²⁺, already present in the original crystallographic data)—plus these solvating H₂O molecules. The whole system was placed into an orthorhombic simulation box, whose size was 102.86 × 138.14 × 116.91 Å³, and on which periodic boundary conditions were applied. Classical molecular dynamics simulations using the AMBER force field^{28,32} were performed to attain thermal equilibrium, and an adiabatic mapping approach³³ was adopted to reconstruct the potential energy hypersurface and to locate the starting configuration for

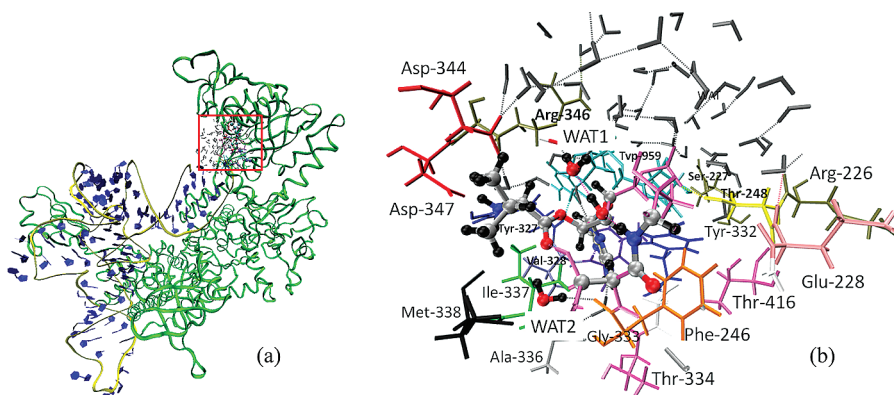


Figure 2. (a) Equilibrated LeuRS (solvating water not shown). The leucyl protein is shown as a green ribbon, the tRNA^{Leu} is shown as a yellow double-stranded tube with the base pairs in blue, and the red square indicates the editing domain where QM atoms were selected. (b) Details of the QM system surrounded by the closest residues. QM atoms are shown as thick sticks and balls, where the color code, here and in all the following figures, is black for H, gray for C, blue for N, red for O, and yellow for P. The surrounding MM residues, within a radius of 10 Å, are colored as follows: red for Asp, purple for Thr, pink for Glu, brown for Arg, orange for Gly, yellow for Ser, green for Ile, light blue for Val, blue for Tyr, and black for Met.

QM/MM metadynamics simulations.²⁸ During this simulation stage, two crucial water molecules, not originally present in the pristine PDB structure and indicated as WAT1 and WAT2 in Figure 2, were shown to approach the catalytic site and identified as potentially involved in the editing reaction in ref 28. Following these results, the LeuRS equilibrated system used in the present work is shown in Figure 2a and presents these two water molecules, WAT1 and WAT2, included in the quantum mechanics subsystem in view of their potential activity as nucleophilic attack catalysts for the hydrolysis reaction as discussed elsewhere.²⁸ In our hybrid quantum mechanics/molecular mechanics (QM/MM) simulations, the QM subsystem was chosen to be the part of the 3'-terminal of tRNA^{Leu} which includes the last phosphate, the ribose ring, and its guanine base, along with the branch representing the leucyl-tRNA connection. Furthermore, we included the threonine (Thr-247) which is rather close to this moiety, forms H-bonds with it, and could be potentially involved in the editing reaction. As pointed out in ref 28, the nucleophilic water molecules WAT1 and WAT2 approach the catalytic site and become active through the formation of a low-barrier hydrogen bond (LBHB). Hence, they become part of the quantum subsystem in the present work. This gives a QM system amounting to 63 atoms, shown in panel b of Figure 2. Since covalent bonds are cut in this selection process, the QM valence was restored by adding five monovalent link atoms.

2.2. QM/MM Approach. In all the simulations presented here, we adopted a hybrid QM/MM approach which has already been shown to be particularly successful in a wealth of biological systems.^{34–43} Specifically, starting from the solvated LeuRS structure described in the previous paragraph and equilibrated at 300 K, we continued for about 8.5 ps the dynamical simulation within our QM/MM setup in which the QM driver is based on the density functional theory⁴⁴ (DFT) within the HCTH gradient-corrected approximation³⁸ for the exchange and correlation functionals. This particular choice has already been extensively used in several biomolecules including phosphates,^{39,40,45–48} and its accuracy is comparable to the hybrid (but computationally more expensive) B3LYP functional. As a first principles molecular dynamics algorithm, we adopted the Car–Parrinello method⁴⁹ as implemented in the CPMD code.⁵⁰ The interaction between core and valence electrons was described by Martins–Troullier pseudopotentials,⁵¹ and the Kohn–Sham orbitals, representing

the valence electrons, were expanded in a plane wave (PW) basis set with an energy cutoff of 70 Ry, with the Brillouin zone sampling restricted to the Γ point. Since the QM subsystem is contained in a subcell of $17 \times 15 \times 21 \text{ \AA}^3$, such a cutoff corresponds to 164 759 PWs, which translates into a mesh of $180 \times 144 \times 216$ points in real space. The QM subsystem is coupled to the MM one according to a full Hamiltonian scheme,^{52,53} which make use of a restrained electrostatic potential (R-ESP) to reduce the computational cost of the particle-mesh Coulomb interaction between the embedded QM subsystem and all the atoms of the outer MM region.

All dynamical simulations were performed at 300 K, and the temperature was controlled via a Nosé–Hoover^{54,55} thermostat on the ionic degrees of freedom. A fictitious electron mass of 380 au and an integration step of 4 au (0.096 fs) ensured a good control of the adiabaticity.⁵⁶

2.3. Reaction Path Sampling. The reaction path was sampled both by metadynamics^{57,58} and Blue Moon⁵⁸ approaches. In the first case we added to the Car–Parrinello Lagrangean, L^{CP} , the degrees of freedom of selected collective variables, $s_\alpha(t)$, plus a history dependent penalty potential $V(s_\alpha, t)$

$$L = L^{\text{CP}} + \sum_{\alpha} \frac{1}{2} M_\alpha \dot{s}_\alpha^2(t) - \sum_{\alpha} \frac{1}{2} k_\alpha [s_\alpha(\mathbf{q}) - s_\alpha(t)]^2 - V(s_\alpha, t) \quad (1)$$

where \mathbf{q} indicates a set of variables (e.g., atomic positions) suitable to describe analytically the reaction coordinates. The fictitious masses for the kinetic term have been set to $M_\alpha = 22.0$ au, and the harmonic coupling constants were set to $k_\alpha = 0.24$ au. Further details on the methods adopted here and their assessment have been reported in detail elsewhere and can be found in the literature.^{39–42,47,48,60,61} The specific choices of collective variables for each simulation will be given in the next paragraphs, as a support to the discussion. The explicit form of the penalty potential used in this work is a superposition of small Gaussians

$$V(s_\alpha, t) = \int_0^t dt' |\dot{s}(t')| \delta \left[\frac{\dot{s}(t')}{|\dot{s}(t')|} (s - s(t')) \right] A(t') \exp \left[-\frac{(s - s(t'))^2}{2(\Delta s)^2} \right] \quad (2)$$

In each metadynamics run, a new Gaussian contribution was added to $V(s_\alpha, t)$ every 120 steps, corresponding to a time

interval of $\Delta t = 0.01$ ps. The amplitude $A(t')$ was set to $W_t = 0.15$ kcal/mol and the width Δs was fixed to 0.18 (in collective variables units). Since, roughly speaking, the free energy landscapes spanned by the collective variables adopted here are not so different in terms of roughness and barriers, these values are kept unchanged in the various metadynamics simulations unless otherwise specified in the ongoing discussion. In all the simulations presented in the following section, in order to reduce the intrinsic error bar in the free energy surface (FES) reconstruction via metadynamics, we used the average procedure described in ref 62. Namely, after allowing for at least a couple of passages back and forth of the collective variables (as described in ref 39 for the case of QM/MM approaches) from the reactants side to the products side on the FES, we computed the arithmetic average of the penalty potential as

$$F(s_a) = -\frac{1}{t_{\text{simul}} - t_{\text{diff}}} \int_{t_{\text{diff}}}^{t_{\text{simul}}} V(s_a, t) dt \quad (3)$$

where t_{simul} is the total simulation time and t_{diff} is the time at which collective variables start diffusing in all the phase space spanned by the selected $s_\alpha(t)$. The coupling of metadynamics with the QM/MM hybrid approach has already been discussed elsewhere^{37–41} and has been shown to be able to study with appreciable accuracy complicated reactions in biomolecular systems.

In the case of Blue Moon simulations, the (single) reaction coordinate $\xi = \xi(\mathbf{R}_I)$ defined by a given subset of atomic coordinates \mathbf{R}_I was assumed to be a specific distance between two atoms, as will be discussed in the next paragraph, and added to the Car–Parrinello Lagrangean as a holonomic constraint

$$L = L^{\text{CP}} + \lambda_k [\xi(\mathbf{R}_I) - \xi_k] \quad (4)$$

where λ_k is a Lagrange multiplier and ξ_k is a selected value of the reaction coordinate. Upon equilibration of each constraint value, corresponding in our specific cases to about 3 ps simulations for each sampled value of $\xi(\mathbf{R}_I)$, the average constraint force f_ξ was computed as time average

$$f_\xi = \langle \lambda_k \rangle_t = \frac{\partial F}{\partial \xi} \quad (5)$$

and the free energy profile is obtained according to the standard thermodynamic integration technique

$$\Delta F = \int_{\xi_0}^{\xi_f} f_\xi d\xi \quad (6)$$

from the initial value ξ_0 to the final one ξ_f .

3. RESULTS AND DISCUSSION

3.1. Hybrid QM/MM Molecular Dynamics. Before performing any reactive simulation, we first did a pre-equilibration of the system starting a QM/MM simulation from the structure obtained after the classical AMBER³² simulation. This hybrid molecular dynamics run lasted for 8.5 ps and allowed also for the newly added electronic degrees of freedom to reach a dynamical equilibrium within the Car–Parrinello framework.

As shown in the upper panel of Figure 3, the thermal equilibrium of the system was attained rather quickly, in about 1–2 ps. However, the structural equilibration took a longer time, namely about 6.5 ps. The root-mean-square displacement (rmsd) was computed during the dynamical simulation by considering all the

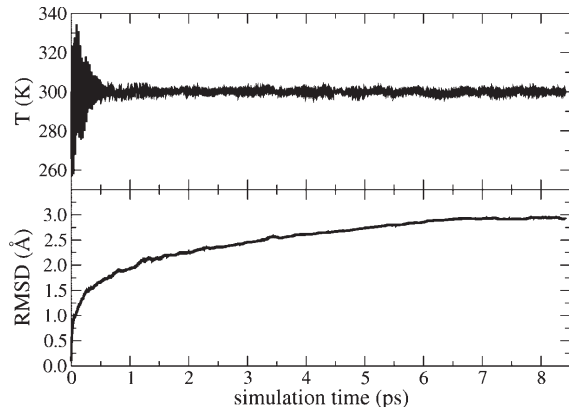


Figure 3. Temperature and root-mean-square displacement (rmsd) of all the heavy atoms of the LeuRS system in solution, as a function of the simulation time, during the QM/MM equilibration phase.

heavy atoms (i.e., H excluded), these atoms being the only ones crystallographically detected. The result is reported in the lower panel of Figure 3. The larger contribution to the rmsd comes from the reorganization of the solvent water, the most mobile species. It is worthy of note to observe that the final equilibrated rmsd does not exceed the experimental resolution,^{11,12} thus being still compatible with the crystallographic data.

The water molecules that in a former simulation were found to come close to the catalytic site of the LeuRS editing domain, as a consequence of a LBHB mechanism,²⁸ do not escape away during the equilibration phase. On the contrary, they are kept in place by relatively long-living H-bonds. These bonds are indicated as HB1 and HB2 in panel a of Figure 4, and their evolution in terms of interatomic distances $O^{\text{WAT1}}-\text{O}^{3'}$ and $O^{\text{WAT2}}-\text{O}$ is shown in panel b of this same figure, where the atoms labeling adopted hereafter is reported.

The quantum approach used in the present study has been extensively benchmarked over the years to characterize aqueous solutions; in particular both in pure water⁶¹ and in salt solutions at biological concentrations,⁶³ the oxygen–oxygen radial distribution function shows a first minimum located at about 3.3 Å, which defines the typical H-bond distance. In the present case, the distances $O^{\text{WAT1}}-\text{O}^{3'}$ and $O^{\text{WAT2}}-\text{O}$ are most of the time below that threshold, indicating that these H-bonds are rather stable. They can be temporarily broken, as observed during the QM/MM simulation, mostly because the 3'-OH group can rotate relatively easily, as will be discussed in the next paragraph, around the $C^3-\text{O}^{3'}$ bond, where C^3- belongs to the ribose of the 3'-terminal of the tRNA^{Leu}. However, their average lifetimes are 3.0 ± 0.7 ps for HB1 and 1.2 ± 0.4 ps for HB2. Despite the poor statistics due to the rather short equilibration time, the lifetime of HB1 is longer than HB2, which, instead, is characterized by a lifetime typical of regular H-bonds (~ 1 ps) in liquid water.⁶⁴ From these considerations, we can infer that a H-bond strength of 3–4 kcal/mol⁶⁵ characterizes HB2, and most likely this value is just a lower bound for HB1.

This H-bonding environment keeps these water molecules trapped in proximity of the active site and seems to suggest that they might play an active role in the reaction mechanism. In particular, the water molecule labeled as WAT1 can go very close to the $-\text{C}^*-\text{O}^*$ moiety, where the catalytic reaction is expected to occur. This was observed also in our classical AMBER simulations, where the minimum distance observed was 2.38 Å. Indeed,

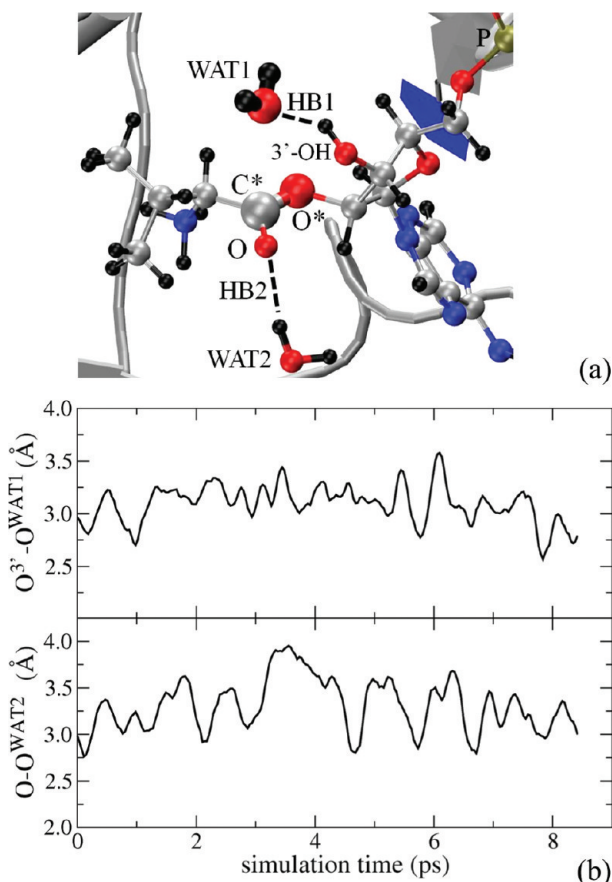


Figure 4. (a) Main atoms of the active site of the editing domain in LeuRS and two water molecules WAT1 and WAT2 trapped in the vicinity of this site, along with their hydrogen bonds indicated as HB1 and HB2. Atoms colors are identical to Figure 2. (b) Evolution of these two H-bonds during the QM/MM dynamical simulation.

water molecules trapped in the vicinity of catalytic sites are not uncommon in biological systems, and often they turn out to trigger the reaction.^{28,38–40,48} Moreover, trapping phenomena at the editing site, although for larger molecules and in particular for antifungal agents, have recently been observed in LeuRS.⁶⁶ Also in that case, an active participation of the $3'$ -OH group of the $3'$ -terminal adenosine of the tRNA^{Leu} was found to be crucial to give rise to the trapping process. This concurs to support the notion that the local environment and the tendency of $2'$ - and $3'$ -OH groups of a general RNA system to form stable H-bonds⁶⁶ with surrounding molecules is a triggering factor in the activation or inhibition of the RNA catalytic activity.²⁸

3.2. Blue Moon Inspection of the Reaction Path. As a first attempt at inspecting the LeuRS editing reaction pathway, a Blue Moon ensemble simulation was performed. In this simulation, the only reaction coordinate used was the distance $C^* - O^{WAT1}$, between the oxygen atom of the closest water molecule, indicated as WAT1 in Figure 4, and the carbon atom labeled as C^* in that same figure. Indeed, the monitoring of the H-bond HB1, discussed in the previous section, seems to suggest that this is a plausible catalytic water molecule prone to promote the reaction. The initial configuration adopted was the QM/MM equilibrated structure, discussed above, and will be used in all the simulations involving free energy sampling explorations described hereafter. Each of the 14 sampled constraint values was equilibrated for

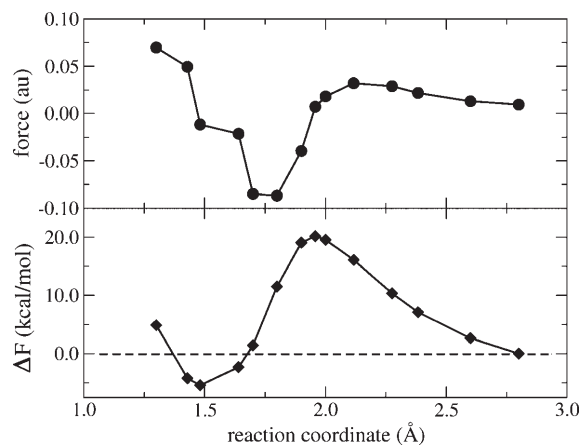


Figure 5. Constraint force (upper panel), in au, and free energy profile (lower panel), in kcal/mol, obtained from the Blue Moon simulation. The sampled reaction coordinate is the distance between the O atom of WAT1 and the C^* atom of the active center at the editing site of the LeuRS system. Filled circles and corresponding diamonds indicate the sampled values of the reaction coordinate, while continuous lines are intended only as a guideline to the eye.

about 3 ps before shrinking the distance, thus amounting to a total simulation time of 42 ps. The thermodynamic integration was performed as described in the computational approach section. The time required by the constraint force to attain the equilibrium after each shrinking of the distance $C^* - O^{WAT1}$ was about 0.5–0.6 ps; therefore, this initial part of the constrained dynamics was discarded in the calculation of time averages. The sampling was refined in proximity of $C^* - O^{WAT1}$ distances that were observed to correspond to transition states and final products, in order to improve the statistics and to avoid missing crucial events.

The result of this simulation is summarized in Figure 5, where the upper panel refers to the constraint force, given by the time average of the Lagrange multiplier, and the lower panel to the free energy profile. Namely, upon dissociation, WAT1 passes across a transition state in which one of its protons becomes shared between WAT1 and $O^{3'}$, corresponding to a value of 2.0 Å of the reaction coordinate. Then the simultaneous formation of the $C^* - O^{WAT1}$ bond and the cleavage of the $C^* - O^*$ bond occur, with the detached proton H^{WAT1} eventually stabilizing as $O^* - H^{WAT1}$. The free energy barrier estimated from this simulation is about 20 kcal/mol. Further structural details will be given in the discussion of the metadynamics simulations because of the close similarity with one of the reaction pathways found there.

Despite the fact that such a reaction pathway and the order of magnitude of the associated free energy barrier are in line with the known experimental outcome,^{1–15} a single reaction coordinate is generally insufficient to accurately keep account of all the slowly varying degrees of freedom of such a complex reaction, as extensively discussed in all the literature (part of which is cited in the references provided here). Thus, in order to complement and improve the results of the Blue Moon analysis, several metadynamics simulations were done to get a better insight into the microscopic mechanism of the LeuRS editing reaction.

3.3. Metadynamics Inspection of the Reaction Path. From the QM/MM equilibrated structure, as mentioned in the previous section, we started metadynamics simulations assuming as a catalytic trigger the dissociation of the water molecule indicated as WAT1

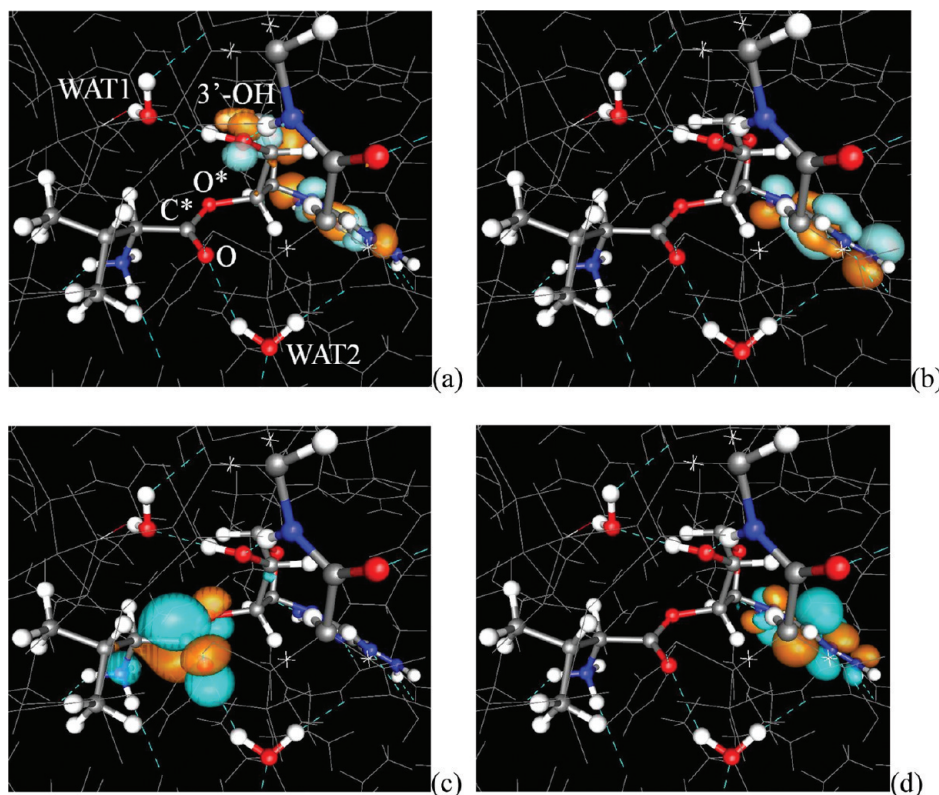


Figure 6. Electronic KS wave functions of the system around the energy gap: (a) HOKS-1, (b) HOKS, (c) LUOKS, and (d) LUOKS+1. The first unoccupied state is localized on the $-C^*-O^*$ bond and ready to accept electrons from the nearby WAT1 H_2O molecule. Wave functions are represented as isosurfaces at $5 \times 10^{-2} 1/\text{Å}^{3/2}$, with positive amplitudes in cyan and negative amplitudes in orange. The color code of the main atoms, represented by sticks and balls, is the same as in previous figures with the exception of H (white). For the sake of clarity, main atoms are labeled only in panel a. Thin gray sticks are the surrounding MM system and dashed blue lines hydrogen bonds.

in Figure 4. This choice was driven by structural and electronic considerations. On one hand, this H_2O molecule is the closest to the active site and its dipole moment is, on average, pointing directly toward the $-C^*-O^*$ bond, the one expected to undergo the cleavage reaction. On the other hand, an accurate analysis of the local electronic structure of the system at the end of the QM/MM equilibration has shown that the electronic states of the Kohn-Sham (KS) Hamiltonian³⁷ close to the energy gap ($E_{\text{gap}} = 2.85$ eV), hence the ones directly involved in the reaction, present the features summarized in Figure 6.

Namely, the highest occupied KS (HOKS) wave function—assumed as a reference level—and the one immediately below (HOKS-1), at -0.37 eV are mainly bonding states of the base of the 3'-terminal adenosine of the tRNA^{Leu}, with considerable amplitudes also on the 3'-OH group, as shown in panels a and b of Figure 6. Above the HOKS, the lowest unoccupied KS (LUOKS) state, energetically located at $+2.85$ eV above HOKS, shows large (antibonding) amplitudes on top of the $-C^*-O^*$ and $-C^*=O$ bonds, with nodes of the wave functions passing across both bonds. This empty state is ready to accept electrons from the WAT1 and to start the reaction, as we observed in the reactive simulations described in the ongoing discussion. Finally, the state above LUOKS (LUOKS+1) is an antibonding state, localized on the base of the 3'-terminal adenosine of the tRNA^{Leu}, but energetically located above LUOKS by about 0.8 eV, thus much higher in energy and unlikely to take an active role in the reaction.

A first metadynamics simulation was performed by using two collective variables, $s_1 = |C^*-O^{\text{WAT1}}|$ and $s_2 = |O^*-H^{\text{WAT1}}|$.

These are the distances between the O atom of the water molecule WAT1 and the carbon atom indicated as C^* in Figure 4 and the distance of one of the H atoms of WAT1 from the O^* atom of the $-C^*-O^*$ moiety, representing the attachment of the tRNA to the Leu protein.

The simulation was actually repeated twice, selecting each time, alternatively, one of the two H atoms of WAT1, leading to identical results. The free energy landscape provided by this simulation is shown in Figure 7.

Starting from the initial local minimum, indicated as panel a in Figure 7 and represented by the equilibrated LeuRS editing site shown in Figure 8a, along this pathway the dissociation of the water molecule WAT1 is promoted by the overlap of the bonding orbitals of this molecule with the LUOKS localized on top of the

$-C^*-O^*$ group. The dissociation of the water molecule into a proton and a hydroxyl anion HO^- occurs in a concerted way with the cleavage of the C^*-O^* bond and the subsequent formation of the C^*-OH^{WAT1} bond (panels b and c of Figure 8). These processes, in fact, occur at a given value of the time-dependent penalty potential $V(s_{\omega}, t)$, before any new Gaussian function is added, and we recall that metadynamics is an energetically ordered (dynamical) exploration of the free energy surface but does not necessarily reproduce time-ordered trajectories.^{57,58,60,61}

According to this reaction pathway, the reactant (Figure 8a) has to overcome a free energy barrier $\Delta F = 19$ kcal/mol to reach the transition state, represented by the dissociation of the H_2O molecule WAT1 and the simultaneous cleavage of the

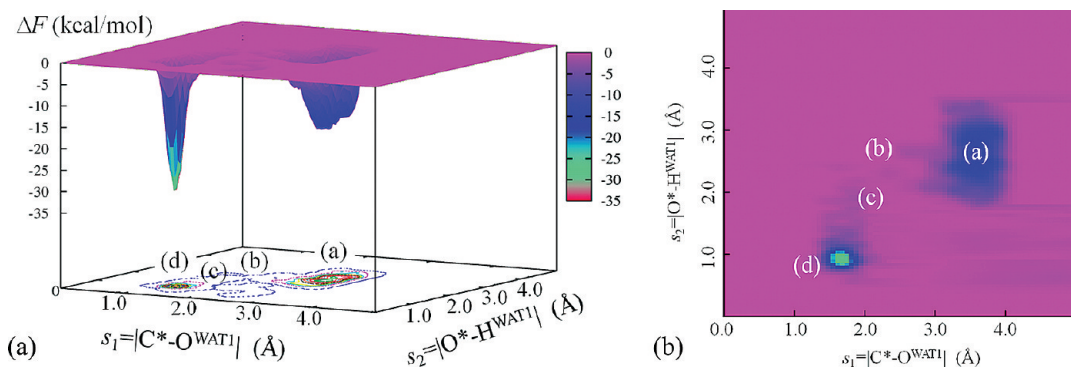


Figure 7. Free energy landscape obtained from the metadynamics simulation of the LeuRS system (panel a) and its two-dimensional contour density version (panel b), assuming as reaction coordinates the distances $C^* - O^{WAT1}$ and $O^* - H^{WAT1}$, the atom labeling being the one given in Figure 4. Labels from (a) to (d) refer to the configurations reported in Figure 8.

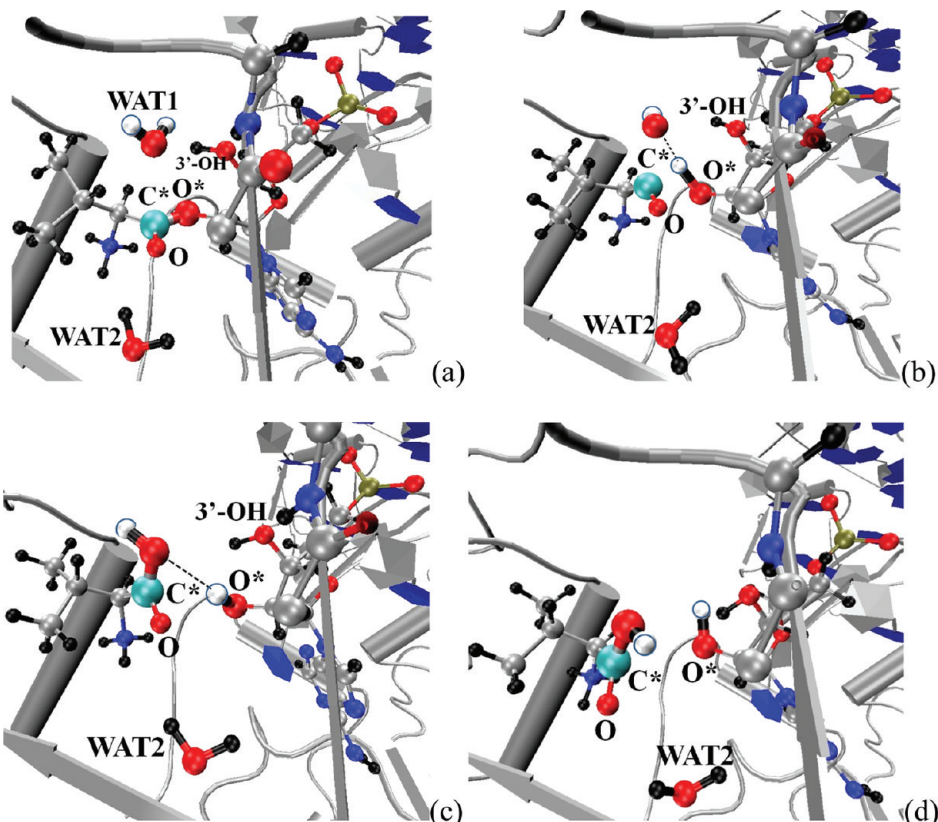


Figure 8. Main steps of the reaction path for the hydrolysis reaction at the editing site of LeuRS. The label of each panel refers to the points on the free energy surface indicated in the previous figure. All the main atoms involved in the reaction are labeled. The color code is the same as in the preceding figures apart from the protons of WAT1 (white circled in blue) and the reactive carbon C* (cyan), evidenced for the sake of clarity.

$-C^*-O^*$ bond. During this phase, the proton detached from WAT1 wanders about, jumping back to WAT1, forming H-bonds with $O^{3'}$, but spending most of the time on O^* , on which eventually stabilizes as shown in panels b, c, and d of Figure 8. A short living (about 1 ps) hydrogen bond is formed between $-O^* - H^{WAT1}$ and $-C^* - O^{WAT1} - H^{WAT1}$ (Figure 8c) which, however, is not present in the final product (Figure 8d). Such a final product turns out to be more stable than the initial reactant by about 8 kcal/mol, thus making at least this stage of the editing reaction a one-directional process along the reaction path. A noticeable feature, at this point, is the close similarity of the free

energy barrier, with respect to the Blue Moon result; however, a structurally different transition state was found, since no shared proton between WAT1 and $O^{3'}$ is realized in the concerted process described above.

An identical simulation, performed using WAT2 instead of WAT1, gave rise to a destabilization and eventually a rupture of the system and resulted in an inconsistent reaction pathway with an unreasonably high free energy barrier, larger than 40 kcal/mol, as expected whenever a wrong reaction path is sampled.⁶⁷ The dissociation of the water molecule is much more problematic, and no contribution from the $3'$ -OH group comes into play to

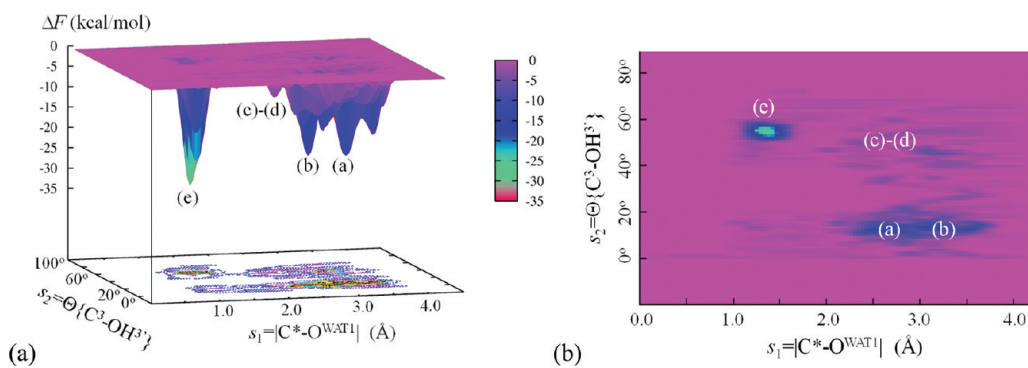


Figure 9. Free energy landscape as obtained from the metadynamics simulation of the LeuRs systems assuming as reaction coordinates the distance $C^* - O^{WAT1}$ and the rotation angle of the 3'-OH group around its $C^3 - O^{3'}$ axis. Labels from a to e refer to the configurations reported in Figure 10. Panel a shows the three-dimensional surface and panel b the corresponding two-dimensional contour density.

promote or help the reaction. The whole sequence of chemical bonds connecting the leucyl protein and the tRNA^{Leu}, from C^* to the ribose ring, undergoes unrealistic distortions, and the final product is just an unrecoverable broken system. This is, however, a clear indication that WAT1 is the right catalytic water molecule.

In the metadynamics inspection of the reaction pathway involving WAT1, we observed that, during the reaction, the 3'-OH group rotates rather freely around its axis represented by the $C^3 - O^{3'}$ bond, C^3 being the carbon atom of the ribose ring of tRNA^{Leu} to which $O^{3'}$ is chemically bonded. This seems to suggest that little or no barrier exists for this specific rotation. Indeed, this is not in contradiction with the trend observed during the QM/MM equilibration phase and summarized in Figure 4, where the H-bond, labeled as HB1, between WAT1 and the 3'-OH group can be temporarily broken and then formed again. Yet, it is difficult to infer something more precise about the rotation barrier on the basis of this simulation. Another questionable point is the protonation of O^* , shown in the final configuration (Figure 8d). In fact, since we made use of the distance $O^* - H^{WAT1}$ as a collective variable a biasing could have been introduced, thus forcing one of the protons of WAT1 to approach O^* . In order to verify whether or not our choice of reaction coordinates biased the reaction, we repeated the simulation using as new set of collective variables the distance $C^* - O^{WAT1}$, as in the former simulations, and the rotation angle of the 3'-OH group around its $C^3 - O^{3'}$ axis, i.e., $s_1 = |C^* - O^{WAT1}|$ and $s_2 = \Theta\{-C^3 - OH^{3'}\}$. The angle of the second collective variable is measured assuming as a reference configuration $s_2 = 0^\circ$ the initial (equilibrated) structure shown in Figure 4a. No other constraints are imposed on the two H of WAT1, which are thus free to move around. Also in this case, the simulation was started from the structure obtained at the end of the QM/MM equilibration phase, prior to the addition of any constraint. The result of this metadynamics simulation is summarized in the free energy landscape of Figure 9. The overall free energy barrier for the reaction is about 18 kcal/mol, slightly lower than the former result, but similar if we keep into the error bar of about 1–2 kcal/mol typical of DFT numerical approaches. The product is more stable than the reactant by about 6–7 kcal/mol, and the labels from a to e in Figure 9 correspond to the main stages of the reaction represented by the configurations, labeled in the same way, shown in Figure 10.

At a first glance, the reactant and the product of this second simulation look identical to the former ones. In fact, although unconstrained, one of the protons of WAT1, upon dissociation

into H^+ and OH^- , is eventually donated to the O^* oxygen, whereas the hydroxyl anion reacts with C^* to form a stable $-C^* - OH$ bond. Nonetheless, the pathway of the reaction is significantly different from the previous one and involves more actively the 3'-OH group in a way identical to what was found in the Blue Moon simulation reported in the former paragraph. Namely, by analyzing the metadynamics trajectory, we noticed first that the initial system is able to switch rather freely from configurations a and b shown in Figure 10. These two structures differ in the donor–acceptor configuration of the H-bond between the 3'-OH group and the water molecule WAT1 and correspond to two rotation angles $\Theta\{-C^3 - OH^{3'}\}$ of about 0° and 45° . The difference in the two structures is that in one case (Figure 10a) the H of the 3'-OH group points toward the oxygen of WAT1, whereas in the second case (Figure 10b) one of the H atoms of WAT1 points toward the $O^{3'}$ atom of the 3'-OH group. The system can easily take any one of these configurations by simply rotating the 3'-OH group around the $C^3 - O^{3'}$ axis, which involves the overcoming of a rather small free energy barrier (about 5 kcal/mol), typical of the breaking/formation of an H-bond.⁶⁵

Then the reaction proceeds with an active (chemical) participation of the 3'-OH group, this time identical to what was observed in the case of the Blue Moon ensemble approach. In fact, during the formation of the $C^* - O^{WAT1}$ bond, one of the protons of WAT1 becomes temporarily a shared proton between O^{WAT1} and $O^{3'}$ as shown by panel c of Figure 10. The formation of the new bond and the transitory detachment of the proton from WAT1 are sufficient to weaken the $C^* - O^*$ bond, which is rapidly cleaved as shown in panel d of the same figure. In these conditions, the shared proton departs from the water molecule and $O^{3'}$, going to saturate the broken bond and forming eventually a stable bond with O^* . The shared proton stage and the cleavage of the $C^* - O^*$ bond can be regarded, also in this case, as concerted for the reasons explained above, since they occur at a given value of the time-dependent penalty potential $V(s_{\omega}, t)$, before any new Gaussian function is added.

A first conclusion that can be drawn from these metadynamics (and Blue Moon) studies is that although reactant and products are indistinguishable in all the (successful) reaction mechanisms identified here, at least two alternative reaction pathways exist, both involving the participation of the 3'-OH group, but while in one case only H-bonds are involved, in the second case a temporary formation of chemical bonds is possible. During this phase, one of the protons of the catalytic water becomes a “strongly”

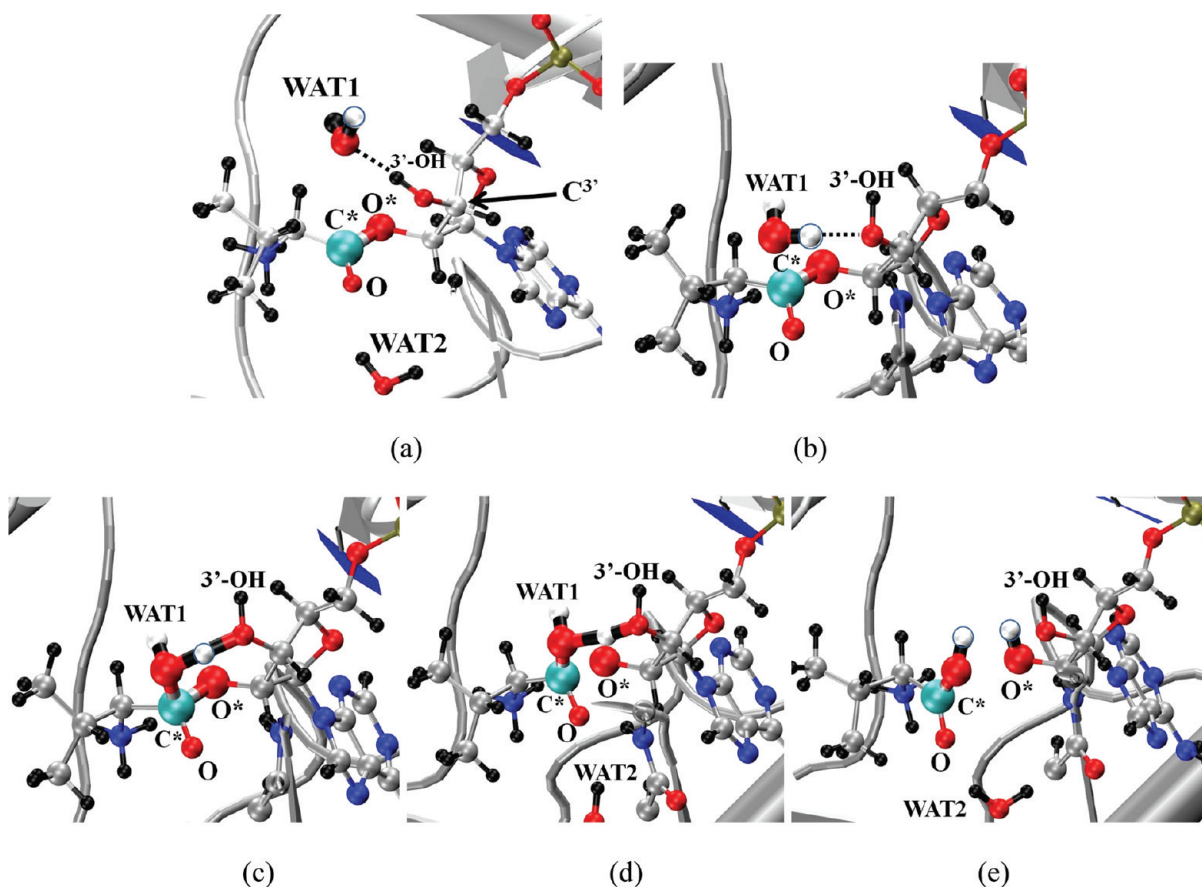


Figure 10. Main steps of the reaction path assuming as reaction coordinates the distance $C^* - O^{WAT1}$ and the rotation of the 3'-OH group. The label of each panel refers to the points on the free energy surface indicated in Figure 8. All the main atoms involved in the reaction are labeled. The color code is the same as in Figure 8.

shared proton, as in an undercoordinated Zundel complex.⁶⁸ At the same time, the rotation barrier for the 3'-OH group is nearly negligible, and the rate-limiting step of the reaction is represented by the concerted dissociation of the catalytic water molecule and the cleavage of the $C^* - O^*$ bond.

4. CONCLUSIONS

By using reactive QM/MM computational approaches, the reaction mechanism and the related energetics in the hydrolysis reaction occurring at the editing domain of the *T. thermophilus* leucyl-tRNA (LeuRS) system has been inspected. On the basis of these simulations, we have shown that the reaction occurring during the enzymatic activity is triggered by a catalytic water molecule, labeled as WAT1, which approaches the catalytic center in proximity of the $-C^* - O^*$ bond connecting the leucyl protein and its cognate tRNA. During this stage, the 3'-OH group of the tRNA^{Leu} forms a stable hydrogen bond with WAT1 and triggers the starting phase of the whole reaction. In fact, although the 3'-OH group is free to rotate around its axis, either the $H^{3'}$ or the $O^{3'}$ atom of this group maintains an H-bond with WAT1, which keeps the water molecule close to the active site. Two possible pathways have been identified, which differ in the role played by the 3'-OH group during the reaction, but that give rise to an identical final product and are characterized by nearly equivalent energy barriers. In the first case the 3'-OH group of the cognate tRNA^{Leu} acts as a Lewis acid, accepting electrons

from WAT1 and helping its dissociation with the resulting OH^- and H^+ and attacking the C^* and O^* atoms, respectively. These two atoms bridging leucyl and tRNA^{Leu} represent the localization sites of the lowest unoccupied (antibonding) atomic orbital, suitable to accommodate electrons. This promotes the bond cleavage process of the reaction and favors the formation of the new bonds mentioned above. In the second case, WAT1 shares a proton with the $O^{3'}$ atom of the 3'-OH group, forming a temporary Zundel-like complex and thus favoring the dissociation of the catalytic water molecule. After its dissociation, the reaction proceeds in the same way summarized above, with a concerted cleavage of the $C^* - O^*$ bond and formation of the $C^* - OH^{WAT1}$ and $O^* - H^{WAT1}$ bonds. This active participation of the 3'-OH group in both the reaction pathways makes its presence an indispensable element in the realization of the enzymatic activity of LeuRS.

■ AUTHOR INFORMATION

Corresponding Author

*E-mail: boero@ipcms.u-strasbg.fr.

■ ACKNOWLEDGMENT

Yohsuke Hagiwara and Masaru Tateno are gratefully acknowledged for providing the configurations of ref 28 used as a starting point for the present set of simulations. Calculations were

performed on the PACS-CS system of CCS—Tsukuba University and partly on the HPC resources of [CCRT/CINES/IDRIS] under the allocation x2010096092 made by GENCI (Grand Equipement National de Calcul Intensif). Insightful discussions with Dino Moras, Alberto D. Podjarny, Isabelle M. Billas, Carlo Massobrio, and Kiyoyuki Terakura are also warmly acknowledged.

■ REFERENCES

- (1) Cusack, S.; Hartlein, M.; Leberman, R. *Nucleic Acids Res.* **1991**, *19*, 3489–3498.
- (2) Nagel, G. M.; Doolittle, R. F. *Proc. Natl. Acad. Sci. U.S.A.* **1991**, *88*, 8121–8125.
- (3) Delarue, M. *Curr. Opin. Struct. Biol.* **1995**, *5*, 48–55.
- (4) Iba, M.; Soll, D. *Annu. Rev. Biochem.* **2000**, *69*, 617–650.
- (5) Hendrickson, T. L.; Schimmel, P. In *Transfer RNA-Dependent Amino Acid Discrimination by Aminoacyl-tRNA Synthetase*; Lapointe, J. P. D., Brakier-Gingras, L., Eds.; Landes Bioscience/Eurekah.com: Austin, TX, 2003; pp 34–64.
- (6) Schimmel, P. *Annu. Rev. Biochem.* **1987**, *56*, 125–158.
- (7) Rao, S. T.; Rossmann, M. G. *J. Mol. Biol.* **1973**, *76*, 241–250.
- (8) Xu, M.-G.; Chen, J.-F.; Martin, F.; Zhao, M.-W.; Eriani, G.; Wang, E.-D. *J. Mol. Biol.* **2002**, *277*, 41590–41596.
- (9) Cavarelli, J.; Delagoutte, B.; Eriani, G.; Gangloff, J.; Moras, D. *EMBO J.* **1998**, *17*, 5438–5448.
- (10) Silvian, L. F.; Wang, J.; Steitz, T. A. *Science* **1999**, *285*, 1074–1077.
- (11) Fukai, S.; Nureki, O.; Sekine, S.; Shimada, A.; Tao, J.; Vassylyev, D. G.; Yokoyama, S. *Cell* **2000**, *103*, 793–803.
- (12) Fukunaga, R.; Yokoyama, S. *J. Mol. Biol.* **2005**, *346*, 57–71.
- (13) Fukunaga, R.; Yokoyama, S. *Nat. Struct. Chem. Biol.* **2005**, *12*, 915–922.
- (14) Tukalo, M.; Yaremchuk, A.; Fukunaga, R.; Yokoyama, S.; Cusack, S. *Nat. Struct. Chem. Biol.* **2005**, *12*, 923–930.
- (15) Fukunaga, R.; Yokoyama, S. *Biochemistry* **2007**, *46*, 4985–4996.
- (16) The anticodon region of tRNA is a sequence of three bases complementary to the codon region of the mRNA (mRNA); the codon and anticodon bases are bonded together by appropriate hydrogen bonds in a double-stranded RNA structure.
- (17) Schmidt, E.; Schimmel, P. *Science* **1994**, *264*, 265–267.
- (18) Lin, L.; Hale, S. P.; Schimmel, P. *Nature* **1996**, *384*, 33–34.
- (19) Lin, L.; Schimmel, P. *Biochemistry* **1996**, *35*, 5596–5601.
- (20) Chen, J. F.; Guo, N. N.; Li, T.; Wang, E. D.; Wang, Y. L. *Biochemistry* **2000**, *39*, 6726–6731.
- (21) Fukunaga, R.; Fukai, S.; Ishitani, R.; Nureki, O.; Yokoyama, S. *J. Biol. Chem.* **2004**, *279*, 8396–8402.
- (22) Cura, V.; Olieric, N.; Guichard, A.; En-Duo, W.; Moras, D.; Eriani, G.; Cavarelli, J. *Acta Crystallogr.* **2005**, *F61*, 899–901.
- (23) Rho, S. B.; Lincecum, T. L.; Martins, S. A. *EMBO J.* **2002**, *21*, 6874–6881.
- (24) Martinis, S. A.; Hsu, J. L. *J. Mol. Biol.* **2008**, *376*, 482–491.
- (25) Eriani, G.; Delarue, M.; Poch, O.; Gangloff, J.; Moras, D. *Nature* **1990**, *347*, 203–206.
- (26) Hagiwara, Y.; Nureki, O.; Tateno, M. *FEBS Lett.* **2009**, *583*, 1901–1908.
- (27) Hagiwara, Y.; Nureki, O.; Tateno, M. *FEBS Lett.* **2009**, *583*, 825–830.
- (28) Hagiwara, Y.; Field, M. J.; Nureki, O.; Tateno, M. *J. Am. Chem. Soc.* **2010**, *132*, 2751–2758.
- (29) Lincecum, T. L., Jr.; Tukalo, M.; Yaremchuk, A.; Mursinna, R. S.; Williams, A. M.; Sproat, B. S.; Van Den Eynde, W.; Link, A.; Van Calenbergh, S.; Grotli, M.; Martinis, S. A.; Cusack, S. *Mol. Cell* **2003**, *11*, 951–963.
- (30) Mursinna, R. S.; Lincecum, T. L., Jr.; Martinis, S. A. *Biochemistry* **2001**, *40*, 5376–5381.
- (31) Zhai, Y.; Martinis, S. A. *Biochemistry* **2005**, *44*, 15437–15443.
- (32) (a) Cornell, W. D.; Cieplack, P.; Bayly, C. I.; Gould, I. R.; Merz, K. M., Jr.; Ferguson, D. M.; Spellmeyer, D. C.; Fox, T.; Caldwell, J. W.; Kollman, P. A. *J. Am. Chem. Soc.* **1995**, *117*, 5179–5197. (b) Case, D. A.; Cheatham, T. E.; Darden, T.; Gohlke, H.; Luo, R.; Merz, K. M.; Onufriev, A.; Simmerling, C.; Wang, B.; Woods, R. J. *J. Comput. Chem.* **2005**, *26*, 1668–1688.
- (33) The adiabatic mapping consists of a set of geometry optimizations performed after short molecular dynamics runs on different configurations, sampled along a reactive trajectory for a set of fixed reaction coordinate(s) as explained in Hagiwara, Y.; Ohta, T.; Tateno, M. *J. Phys.: Condens. Matter* **2009**, *21*, 064234.
- (34) Gervasio, F. L.; Carloni, P.; Parrinello, M. *Phys. Rev. Lett.* **2002**, *89*, 108102.
- (35) Carloni, P.; Röthlisberger, U.; Parrinello, M. *Acc. Chem. Res.* **2002**, *35*, 455–464.
- (36) Colombo, M. C.; Guidoni, L.; Laio, A.; Magistrato, A.; Maurer, P.; Piana, S.; Rohrig, U.; Spiegel, K.; Sulpizi, M.; VandeVondele, J.; Zumstein, M.; Röthlisberger, U. *Chimia* **2002**, *56*, 13–19.
- (37) Magistrato, A.; De Grado, W. F.; Laio, A.; Röthlisberger, U.; VandeVondele, J.; Klein, M. L. *J. Phys. Chem. B* **2003**, *107*, 4182–4188.
- (38) von Lilienfeld, O. A.; Tavernelli, I.; Röthlisberger, U.; Sebastiani, D. *J. Chem. Phys.* **2005**, *122*, 014133.
- (39) Boero, M.; Ikeda, T.; Ito, E.; Terakura, K. *J. Am. Chem. Soc.* **2006**, *128*, 16798–16807.
- (40) Dal Peraro, M.; Ruggerone, P.; Raugei, S.; Gervasio, F. L.; Carloni, P. *Curr. Opinion Struct. Biol.* **2007**, *17*, 149–156.
- (41) Gervasio, F. L.; Boero, M.; Parrinello, M. *Angew. Chem., Int. Ed.* **2006**, *45*, 5606–5609.
- (42) Boero, M.; Gervasio, F. L.; Parrinello, M. *Mol. Simul.* **2007**, *33*, 57–60.
- (43) Boero, M.; Park, J. M.; Hagiwara, Y.; Tateno, M. *J. Phys.: Condens. Matter* **2007**, *19*, 365217.
- (44) Kohn, W.; Sham, L. *J. Phys. Rev.* **1965**, *140*, A1133–A1138.
- (45) Hamprecht, F. A.; Cohen, A. J.; Tozer, D. J.; Handy, N. C. *J. Chem. Phys.* **1998**, *109*, 6264–6271.
- (46) Boese, A. D.; Doltsinis, N. L.; Handy, N. C.; Sprik, M. *J. Chem. Phys.* **2000**, *112*, 1670–1678.
- (47) Gervasio, F.; Laio, A.; Iannuzzi, M.; Parrinello, M. *Chem.—Eur. J.* **2004**, *10*, 4846–4852.
- (48) Boero, M.; Tateno, M.; Terakura, K.; Oshiyama, A. *J. Chem. Theory Comput.* **2005**, *1*, 925–934.
- (49) Car, R.; Parrinello, M. *Phys. Rev. Lett.* **1985**, *55*, 2471–2474.
- (50) CPMD, version 3.13.1; <http://www.cpmd.org>; Copyright IBM Corp. 1990–2011; Copyright MPI für Festkörperforschung Stuttgart, 1997–2001.
- (51) Troullier, N.; Martins, J. L. *Phys. Rev. B* **1991**, *43*, 1993–2006.
- (52) Laio, A.; VandeVondele, J.; Röthlisberger, U. *J. Chem. Phys.* **2002**, *116*, 6941–6947.
- (53) Laio, A.; VandeVondele, J.; Röthlisberger, U. *J. Phys. Chem. B* **2002**, *106*, 7300–7307.
- (54) (a) Nosé, S. *Mol. Phys.* **1984**, *52*, 255–268. (b) Nosé, S. *J. Chem. Phys.* **1984**, *81*, 511–519.
- (55) Hoover, W. G. *Phys. Rev. A* **1985**, *31*, 1695–1697.
- (56) Grossman, J. C.; Schwegler, E.; Draeger, E. W.; Gygi, F.; Galli, G. *J. Chem. Phys.* **2004**, *120*, 300–311.
- (57) Laio, A.; Parrinello, M. *Proc. Natl. Acad. Sci. U.S.A.* **2002**, *99*, 12562–12566.
- (58) Iannuzzi, M.; Laio, A.; Parrinello, M. *Phys. Rev. Lett.* **2003**, *90*, 238302.
- (59) Sprik, M.; Ciccotti, G. *J. Chem. Phys.* **1998**, *109*, 7737–7744.
- (60) Laio, A.; Rodriguez-Fortea, A.; Gervasio, F. L.; Ceccarelli, M.; Parrinello, M. *J. Phys. Chem. B* **2005**, *109*, 6714–6721.
- (61) Laio, A.; Gervasio, F. L. *Rep. Prog. Phys.* **2008**, *71*, 126601.
- (62) Silvestrelli, P. L.; Parrinello, M. *J. Chem. Phys.* **2002**, *111*, 3572–3580.
- (63) Schmidt, D. A.; Scipioni, R.; Boero, M. *J. Phys. Chem. A* **2009**, *113*, 7725–7729.
- (64) Bergman, D. L. *Chem. Phys.* **2000**, *253*, 267–282.

- (65) Walrafen, G. E.; Fisher, M. R.; Hokmabadi, M. S.; Yang, W.-H. *J. Chem. Phys.* **1986**, *85*, 6970–6982.
- (66) Rock, F. L.; Mao, W.; Yaremczuk, A.; Tukalo, M.; Crépin, T.; Zhou, H.; Zhang, Y.-K.; Hernandez, V.; Akama, T.; Baker, S. J.; et al. *Science* **2007**, *316*, 1759–1761.
- (67) Kamiya, K.; Boero, M.; Tateno, M.; Shiraishi, K.; Oshiyama, A. *J. Am. Chem. Soc.* **2007**, *129*, 9663–9673.
- (68) Boero, M.; Ikeshoji, T.; Terakura, K. *ChemPhysChem* **2005**, *6*, 1775–1779.